Transportation Research Part D 38 (2015) 144–155

Contents lists available at ScienceDirect

Transportation Research Part D

journal homepage: www.elsevier.com/locate/trd

Ultrafine particle infiltration into passenger vehicles. Part II: Model analysis

Eon S. Lee [a,b], Michael K. Stenstrom [b,c], Yifang Zhu [a,c,*]

[a] Department of Environmental Health Sciences, Jonathan and Karin Fielding School of Public Health, University of California Los Angeles, Los Angeles, CA 90095-1772, USA
[b] Department of Civil and Environmental Engineering, Henry Samueli School of Engineering and Applied Science, University of California Los Angeles, Los Angeles, CA 90095-1593, USA
[c] Institute of Environment and Sustainability, University of California Los Angeles, Los Angeles, CA 90095-1772, USA

ARTICLE INFO

Article history:
Available online 8 December 2014

Keywords:
Ultrafine particle
Model
Infiltration
In-cabin
Passenger
Automobile

ABSTRACT

Experimental studies showed that infiltration and passive ventilation are important air exchange mechanisms inside vehicles but previous mathematical models did not consider either one. In this study, we incorporated infiltration and passive ventilation to advance the existing mathematical models and evaluated how different transport mechanisms affect passenger exposures at increasing speeds. Infiltration was formulated using Bernoulli's equation and passive ventilation was derived empirically. The new model describes ultrafine particle (UFP) and carbon dioxide (CO_2) transport for a wide range of driving speed under any ventilation conditions. Unlike statistical models, this mathematical model can also provide vehicle-specific and transport mechanism-specific information. The model predictions were in a good agreement with data collected from 10 different vehicle models with an average discrepancy of less than 16% for UFPs and less than 3% for CO_2. Under outdoor air (OA) mode, when the fan is off, the model simulation showed that the infiltration and passive ventilation can substantially increase the UFP *I*/*O* (in-cabin/on-road concentrations) ratio from 0.15 at 0 km/h to 0.57 at 130 km/h. At medium fan setting, mechanical ventilation dominates and UFP *I*/*O* stays at 0.58 regardless of driving speed. Under recirculation (RC) mode, infiltration increases and the RC-mode filtration only removed 44% and 69% of the infiltrated particles at the lowest and medium fan settings, respectively. Model simulations under OA mode show that infiltration starts to occur above 115 km/h with the lowest fan setting; whereas, medium and higher fan settings prevent infiltration up to 145 km/h.

Introduction

Recent health studies have raised concerns for ultrafine particles (UFPs, diameter $\leqslant$100 nm) and in-cabin passenger exposures. UFPs are associated with pulmonary (Penttinen et al., 2001; Peters et al., 1997; von Klot et al., 2002) and cardiovascular (Andersen et al., 2010; Stolzel et al., 2007) diseases. UFPs can also increase the risk of systemic inflammation and genetic mutation (Elder et al., 2007; Sioutas et al., 2005; Somers et al., 2004).

* Corresponding author at: Institute of Environment and Sustainability, University of California Los Angeles, Los Angeles, CA 90095-1772, USA. Tel.: +1 310 825 4324; fax: +1 310 794 2106.
E-mail address: Yifang@ucla.edu (Y. Zhu).

http://dx.doi.org/10.1016/j.trd.2014.11.005
1361-9209/

Nomenclature

P	pressure at a given point
v	fluid speed
C_{in}	in-cabin concentration of UFPs (cm^{-3}) or CO_2 (ppm)
C_{out}	ambient concentration of UFPs (cm^{-3}) or CO_2 (ppm)
Q_{vent}	total ventilation airflow rate (m^3/h)
Q_{atvOA}	OA ventilation airflow rate (m^3/h)
Q_{psvOA}	OA passive ventilation airflow rate (m^3/h)
Q_{atvRC}	RC ventilation airflow rate (m^3/h)
Q_{inf}	infiltration airflow rate (m^3/h)
$Q_{Minimum}$	minimum ventilation airflow rate to prevent infiltration (m^3/h)
$Q_{Observed}$	observed ventilation airflow rate (m^3/h)
dP_{mech}	mechanical ventilation-controlled differential pressure (Pa)
dP_{aero}	aerodynamic differential pressure on vehicle envelope surface (Pa)
ΔP_{inf}	differential pressure affecting infiltration (Pa)
AER	overall air exchange rate (h^{-1})
AER_{atvOA}	air exchange rate caused by OA-mode active ventilation (h^{-1})
ρ	density of fluid
g	gravitational acceleration coefficient
h	elevation of a given point
t	time (s)
$v_{driving}$	driving speed (km/h)
V_{cabin}	passenger cabin volume (m^3)
K_f	leakage flow coefficient ($m^3/s\ Pa^n$)
n	leakage pressure exponent (ø)
α	particle penetration loss partitioning coefficient (ø)
β	surface deposition rate of UFPs (h^{-1})
η	cabin air filter efficiency (ø)
E	CO_2 emission rate from passenger exhalation (g/h/person)
K_{psvOA}	passive ventilation coefficient (ø)
F_{rev}	reverse leakage flow correction factor (ø)
K_p	aerodynamic pressure distribution coefficient (ø)
AER_{psvOA}	air exchange rate caused by OA-mode passive ventilation (h^{-1})

Elevated UFP concentrations have been frequently observed on urban roadways (Shi et al., 2003). Even with cabin air filtration under the outdoor air (OA) ventilation mode, the in-cabin UFP concentration is usually an order of magnitude higher than urban background concentration (Morawska et al., 2008). Although recirculation (RC) mode can lower the in-cabin UFP concentration (Pui et al., 2008), our companion study showed that significant infiltration can still occur through trunk gaps (Lee et al., 2015). In-cabin exposure can contribute up to 45–50% of total daily exposure to UFPs (Fruin et al., 2008; Zhu et al., 2007).

Previous studies have proposed mathematical models to estimate passenger exposures to UFPs in vehicles. However, these models often overlooked infiltration because it is poorly understood. For example, a previous study assumed that infiltration is negligible (Pui et al., 2008). Xu and Zhu (2009) improved the approach of Pui et al. (2008) by introducing a quantitative relationship, which eliminates the need to assume negligible infiltration and quantified infiltration using an idealized leakage model (Baker et al., 1987). However, the leakage model of Baker et al. (1987) only works for idealized conditions and requires measurements of complex leakage geometry. Therefore, previous mathematical models are limited for practical applications. Up to date, there is no mathematical model that can fully explain how much infiltration contributes to passenger exposures. Understanding of the effects of infiltration is particularly important for developing exposure mitigation strategies, such as those proposed by Lee and Zhu (2014) and Tartakovsky et al. (2013). The knowledge gap in infiltration has also limited quantitative understanding of the effects of different UFP transport mechanisms on passenger exposures overall.

In addition to the mathematical models discussed above, previous studies have also proposed statistical models to estimate passenger exposure. Hudda et al. (2012) generalized UFP I/O (in-cabin/on-road concentrations) ratios using a statistical regression of vehicle age, driving speed, and fan strength, which allows in-cabin UFP I/O estimation from the easily obtainable parameters. However, the statistical regression method may impose uncertainty across different vehicle models. For instance, this statistical model defines the fan strength using a 0–1 scale and takes the value of 1 for the maximum fan setting, which neglects differences in vehicle makes. In fact, mechanically controlled ventilation airflow rates are highly variable from 200 to 600 m^3/h across different vehicles at the same maximum fan setting (Lee et al., 2015). In addition, this statistical model is limited to reflect vehicle-specific differences such as leakage characteristics, shown in Figs. 2 and 3 of the companion paper

(Lee et al., 2015). Note that leakage characteristics (e.g., leakage geometry) can be different even for the same model vehicles of the same manufacturer if the manufacturer changed their design for different year models.

This study aims to evaluate to what extent different pollutant transport mechanisms affect passenger exposures and how they change at increasing driving speeds. An infiltration term was mathematically derived by using Bernoulli's equation, which describes the balance of pressure energy, kinetic energy, and potential energy for inviscid incompressible fluids (Batchelor, 1967). The derived infiltration term was then coupled with a previously developed in-cabin air quality model (Xu and Zhu, 2009). This new model enables dynamic simulations of in-cabin UFPs as a function of speed under any ventilation conditions at any time and elucidates the effects of infiltration on passenger exposures inside vehicles.

Model development

Modeling parameters

Fig. 1 illustrates the parameters for modeling transport of particle and gas pollutants (e.g., UFP and CO_2) under different ventilation conditions. Different gain/loss mechanisms are used to determine the in-cabin concentration (C_{in}) depending on the model selections for UFPs/CO_2 and OA/RC.

Under the OA mode, the active OA ventilation airflow rate (Q_{atvOA} in Fig. 1a and c) can be measured at each fan setting under the stationary conditions as described in the *Stationary Measurements section* of the companion paper (Lee et al., 2015). The passive ventilation airflow rate (Q_{psvOA}) can be calculated by multiplying the air exchange rate due to OA-mode passive ventilation (AER_{psvOA}) and the passenger cabin volume (V_{cabin}): $Q_{psvOA} = AER_{psvOA} \cdot V_{cabin}$. Regression analyses showed the AER_{psvOA} is a linear function of driving speed ($v_{driving}$, see the Supporting information S1 for more details). This agrees well with results from previous studies of Fletcher and Saunders (1994) and Ott et al. (2008). The sum of the two airflow rates (i.e., $Q_{atvOA} + Q_{psvOA}$ in Fig. 1a) supplies outside air to vehicle cabin under OA mode. The supplied air is filtered by the manufacturer-installed cabin air filter, whose efficiency (η) is approximately 40% in this study. In the passenger cabin, particle loss occurs by the surface deposition described with the deposition rate ($\beta = 8\ h^{-1}$) (Gong et al., 2009) until the cabin air is exhausted through the leakage around the vehicle envelope. Infiltration is modeled with the infiltration airflow rate (Q_{inf}). UFP uptake by passenger inhalation is negligible because the respiratory uptake rate is much smaller than the UFP gain/loss rates due to other mechanisms (Xu and Zhu, 2009).

Under RC mode, the ventilation airflow rate (Q_{atvRC}) replaces both Q_{atvOA} and Q_{psvOA} (Fig. 1b) because there is no outside air intake. RC mode ventilation acts as an UFP sink because cabin air recirculates continuously, repeatedly filtering the air. In this case, UFP penetration takes place only through infiltration. Particle loss during infiltration due to entrapment or retention at the door, windows, and trunk gaps is defined by a penetration loss partitioning coefficient ($\alpha = 0.60$), which was previously measured through bench-scale experiments (Xu et al., 2010).

The CO_2 model is similar to the UFP model and has the same airflow rates (Q_{atvOA}, Q_{psvOA}, and Q_{inf}) under OA mode (as shown in Fig. 1c), but only Q_{inf} is present under RC mode (Fig. 1d). The parameter η disappears because the automotive filtration system does not remove CO_2. Instead, the CO_2 emission rate (E) from passenger exhalation is considered. Table 1

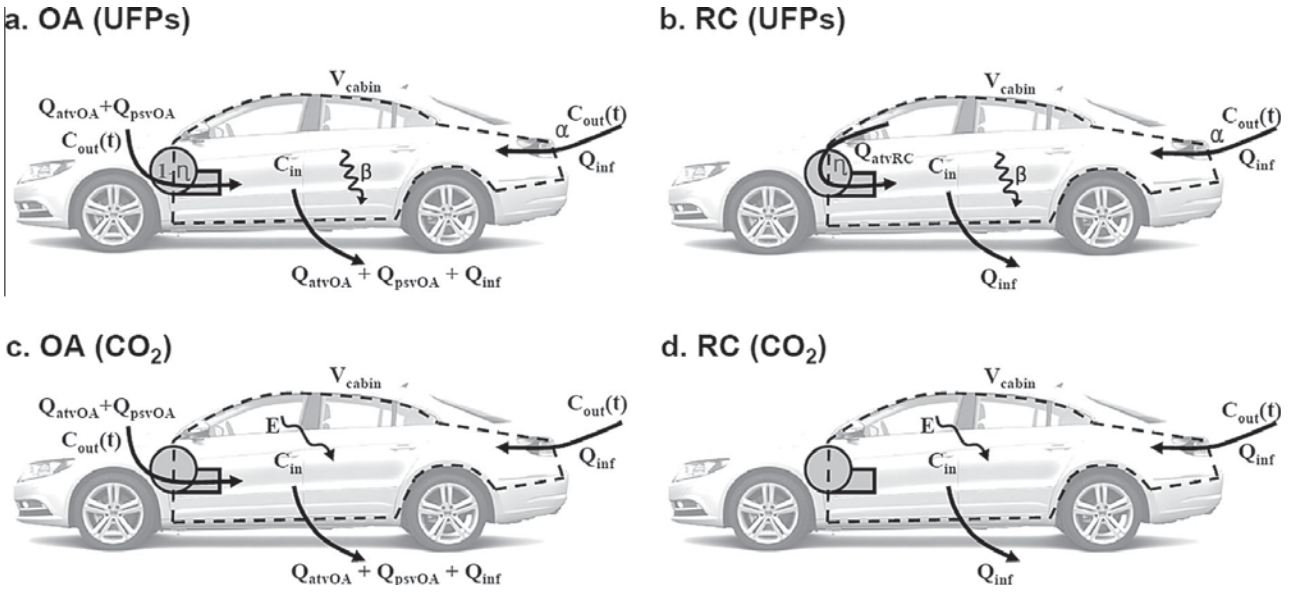

Fig. 1. Graphical illustrations indicate the modeling parameters for UFPs and CO_2 in the same modeling domain (V_{cabin}, dash-line) in the outdoor air (OA) mode (a and c) and the recirculation (RC) mode (b and d). The arrows indicate airflow paths.

Table 1
A summary of the modeling equations for UFPs and CO_2 under different ventilation conditions.

$\frac{dC_{in}}{dt} = S - L \cdot C_{in}$		Source term (S)	Loss term (L)
UFPs	OA	$C_{out}(t) \cdot \left\{(1-\eta) \cdot \left(\frac{Q_{atvOA}+Q_{psvOA}}{V_{cabin}}\right) + \alpha \cdot \frac{Q_{inf}}{V_{cabin}}\right\}$	$\frac{Q_{atvOA}+Q_{psvOA}+Q_{inf}}{V_{cabin}} + \beta$
	RC	$C_{out}(t) \cdot \alpha \cdot \frac{Q_{inf}}{V_{cabin}}$	$\eta \cdot \frac{Q_{atvRC}}{V_{cabin}} + \frac{Q_{inf}}{V_{cabin}} + \beta$
CO_2	OA	$C_{out}(t) \cdot \left(\frac{Q_{atvOA}+Q_{psvOA}+Q_{inf}}{V_{cabin}}\right) + \frac{E}{V_{cabin}}$	$\frac{Q_{atvOA}+Q_{psvOA}+Q_{inf}}{V_{cabin}}$
	RC	$C_{out}(t) \cdot \frac{Q_{inf}}{V_{cabin}} + \frac{E}{V_{cabin}}$	$\frac{Q_{inf}}{V_{cabin}}$

summarizes the modeling equations corresponding to gain and loss mechanisms shown in Fig. 1 for both the OA/RC scenarios and for UFPs or CO_2.

Modeling assumptions

The modeling approach in this study includes three assumptions: well-mixed condition, no temperature difference, and no UFP phase change by coagulation, condensation, and evaporation. The well-mixed condition is a valid assumption when considering high ventilation airflow rates (i.e., up to 600 m^3/h) in a small cabin volume (approximately 3 m^3 for a sedan and 7 m^3 for a minivan). Experimental studies measuring UFP concentrations at different locations inside passenger cabins also support this assumption (Joodatnia et al., 2013; Ott et al., 2008). Negligible temperature effect on in-cabin particle concentration was also confirmed previously (Fletcher and Saunders, 1994).

For simplicity of the model, no phase change is assumed for UFPs. This assumption is justified by the time required for coagulation. Coagulation can take a few hours to reach half of the particle number concentration, for example, 2.6 h for 40-nm particles at 10^5 cm^{-3} concentration (Hinds, 1999). The calculated AER (i.e., $AER_{atvOA} = Q_{atvOA}/V_{cabin}$) was larger than 100 h^{-1}, which means the average particle residence time was much shorter (i.e., ~36 s) than the coagulation time-scale of a few hours. Therefore, the assumption of no particle phase change is expected to have little effect on the observed concentration.

Model formulation: infiltration and passive ventilation

Infiltration airflow rate (Q_{inf}) and passive ventilation airflow rate (Q_{psvOA}) are two important parameters, both change as a function of driving speed. Because infiltration occurs when the mechanical ventilation-controlled pressure in the cabin (dP_{mech}) is lower than the aerodynamic-induced surface pressure on the moving vehicle (dP_{aero}), the infiltration occurs due to the difference between the two competing pressures (i.e., $\Delta P_{inf} = dP_{aero} - dP_{mech}$). Note that the absolute atmospheric pressure subtracts to zero when calculating ΔP_{inf}.

Assuming inviscid incompressible fluid, Bernoulli's equation given in Eq. (1) describes the energy conservation at two points on a streamline (e.g., infiltration).

$$\underbrace{P}_{\text{Pressure Energy}} + \underbrace{\frac{\rho}{2} \cdot v^2}_{\text{Kinetic Energy}} + \underbrace{\rho \cdot g \cdot h}_{\text{Potential Energy}} = \text{Const.} \tag{1}$$

where, P is the pressure at a given point; ρ is the density of fluid; v is the fluid speed; g is the gravitational acceleration coefficient; and, h is the elevation of a given point. In case of infiltration, the *potential energy* is considered negligible at the same elevation; whereas, the *pressure energy* converts to the *kinetic energy*. Thus, the pressure difference (e.g., ΔP_{inf} for infiltration and dP_{mech} for mechanical ventilation) becomes the *kinetic energy* causing a movement of fluid.

Eq. (1) can be rearranged to derive a power-law correlation between mechanical ventilation airflow rate and the pressure difference, as shown in Eq. (2). Ventilation airflow rate (Q_{atvOA}) in OA mode follows the power-law function with respect to mechanically controlled cabin pressure (i.e., dP_{mech}) as follows:

$$Q_{atvOA} = K_f \cdot dP_{mech}^{n} \tag{2}$$

where K_f is the leakage flow coefficient, n is the pressure exponent. K_f and n are vehicle-specific parameters describing envelope leakage characteristics. The values can be obtained from the power-law regression with the measurements of Q_{atvOA} and dP_{mech} in stationary condition (i.e., cabin pressurization test). The experimental methodology is described in details in the Model formulation: infiltration and passive ventilation section *Stationary Measurements* of the companion paper (Lee et al., 2015) and Table 2 summarized K_f and n for the vehicles used for model validation.

When a vehicle is moving, dP_{mech} increases because of passive ventilation airflow rate (Q_{psvOA}) in addition to Q_{atvOA}. By rearranging Eq. (2) for dP_{mech}, Eq. (3) describes the level of cabin pressurization (i.e., dP_{mech}) under driving conditions.

$$dP_{mech} = e^{\frac{1}{n}\ln\left(\frac{Q_{atvOA}+Q_{psvOA}}{K_f}\right)} \tag{3}$$

Table 2
A summary of the test vehicle models used for experimental validation.

ID	Model	Year	Mileage (km)	Cabin volume (m^3)	Flow coefficient (K_f)	Pressure exponent (n)
1	Toyota Prius	2012	9,102	3.28	46.83	0.81
2	Ford Focus	2012	51,347	2.92	18.78	0.82
3	Honda Accord	2011	51,194	3.43	69.39	0.49
4	Hyundai Sonata	2013	21,712	3.28	40.58	0.69
5	Nissan Sentra	2012	30,398	3.11	6.73	0.82
6	Toyota Camry	2012	1,931	3.34	61.49	0.48
7	VW Jetta	2012	14,917	3.11	29.77	0.75
8	Ford Explorer	2013	16,510	4.89	17.66	0.89
9	Toyota Highlander	2012	10,611	4.43	60.09	0.56
10	Toyota Sienna	2011	74,174	5.76	72.12	0.53

Independent from dP_{mech}, the dP_{aero} on the vehicle surface can also take place during driving. The dP_{aero} was experimentally derived from the regression of the continuous measurements of differential pressure at the rear trunk leakage, where the infiltration occurs (Lee et al., 2015). The dP_{aero} is given for a wide range of driving speeds ($v_{driving}$, ranging 0–130 km/h) as follows:

$$dP_{aero} = K_p \cdot a \cdot e^{b \cdot v_{driving}} \tag{4}$$

where K_p is the aerodynamic pressure distribution coefficient. The magnitude of the exponential increase in dP_{aero} is slightly different depending on the aerodynamic design or shape of the vehicle. The two coefficients (i.e., a and b) of Eq. (4) are 0.51 and 0.04 for a sedan and 4.44 and 0.02 for a minivan. The values were experimentally determined in the companion study (see Fig. 5 in Lee et al., 2015).

Q_{atvOA} and Q_{psvOA} in Eq. (3) create a positive cabin pressure (i.e., $dP_{mech} > 0$). However, when $v_{driving}$ in Eq. (4) becomes high enough, it makes ΔP_{inf} positive (i.e., $dP_{aero} > dP_{mech}$) and infiltration occurs. Therefore, infiltration depends on these two competing pressures and ΔP_{inf} can take the following form:

$$\Delta P_{\text{inf}} = \underbrace{K_p \cdot a \cdot e^{b \cdot v_{driving}}}_{dP_{aero}} - \underbrace{e^{\frac{1}{n}\ln\left(\frac{Q_{atvOA}+Q_{psvOA}}{K_f}\right)}}_{dP_{mech}} \tag{5}$$

Previous studies have found that the air exchange rate (AER) due to passive ventilation (AER_{psvOA}) is a linear function of $v_{driving}$ (Fletcher and Saunders, 1994; Ott et al., 2008) as follows:

$$AER_{psvOA} = K_{psvOA} \cdot v_{driving} \tag{6}$$

where K_{psvOA} is the passive ventilation coefficient. Based on experimental observations a best fit value of 0.21 was determined for K_{psvOA}. Note that the vehicle models used to derive K_{psvOA} were different from the vehicle models used for the model validation. This coefficient is in good agreement with previous studies (see Supporting information S1).

Q_{psvOA} is also a linear function of $v_{driving}$ because Q_{psvOA} is equal to the product of AER_{psvOA} and V_{cabin} under well-mixed condition. Thus, under OA mode, both competing pressures (i.e., dP_{aero} and dP_{mech}) depend on the changes in $v_{driving}$ of a moving vehicle. Under RC mode, dP_{mech} is equal to zero regardless of $v_{driving}$ because RC mode ventilation does not pressurize the passenger cabin. Thus, only dP_{aero} determines the differential pressure affecting infiltration (ΔP_{inf}) under RC mode.

With the use of ΔP_{inf}, Q_{inf} is expressed as follows:

$$Q_{\text{inf}} = F_{rev} \cdot K_f \cdot \Delta P_{\text{inf}}^{n} \tag{7}$$

where F_{rev} is the reverse leakage flow correction factor ($F_{rev} = 0.65$) adopted from a previous study (Fletcher and Saunders, 1994). The F_{rev} corrects Eq. (7) for the differences between infiltration and exfiltration. It is important to note that the K_f and n are the parameters acquired from cabin pressurization tests (see Lee et al., 2015) which leads to exfiltration. However, infiltration flow occurs in the reverse direction and experiences higher magnitude of resistance. The infiltration airflow rate was approximately at 65% of exfiltration flow rate (Fletcher and Saunders, 1994). Once again, the relationship must be corrected with F_{rev} because the infiltration flow occurs in the reverse direction.

Model calibration

The aerodynamic surface pressure affecting infiltration (dP_{aero}) is widely distributed along with the trunk gaps (Kang et al., 2012; Song et al., 2012). However, it is not feasible to measure aerodynamic pressures across the wide-spread rear-trunk leakage. In this modeling approach, Eq. (4) was derived from the continuous measurement of dP_{aero} on the lateral-center of the rear trunk gap, where dP_{aero} is the highest. The actual differential pressure affecting infiltration (i.e., ΔP_{inf}) consequently becomes lower than the measurements at the lateral-center. Therefore, the aerodynamic pressure distribution coefficient (K_p) is applied to correct the difference.

Since K_p is not a measureable parameter, the model is calibrated using optimized value of K_p determined from a best fit of measured and calculated CO_2 concentration in the RC-mode. In a moving vehicle under RC mode, infiltration is the only air exchange mechanism triggered by the changes in dP_{aero}. Using the CO_2 data to calibrate the model is advantageous because it does not require a phase change assumption. The parameter best-fit K_p was 0.33 for sedans and 0.23 for minivans, respectively. Finally, the calibrated model was validated with *in-situ* measurements of CO_2 and UFPs collected from 10 different vehicle models listed in Table 2.

Experimental measurements

Table 2 shows a list of vehicle models in which data were collected for model calibration. All test vehicle models were equipped with original equipment manufacturer (OEM) cabin air filters. Under stationary conditions, cabin pressurization test was conducted to estimate the vehicle leakage properties (K_f and n). Mechanical ventilation airflow rates (i.e., Q_{atvOA}) at different fan settings were also measured for model input under stationary conditions. Detailed experimental method and instrument information are described in the *Stationary Measurements* section of the companion paper (Lee et al., 2015).

The model validation data were collected in stationary, local roadway, and freeway environments for at least 15 min in each of the 10 vehicle models. All instruments were set to 1-s sampling intervals. Throughout data collection, all windows were closed and the fan was set to the medium fan setting. The medium fan setting ventilation airflow rate was 306 (±101) m^3/h on average. Ambient temperature and relative humidity were 23 (±4) °C and 50 (±19)%, respectively. In-cabin air temperature and relative humidity were 21 (±3) °C and 70 (±6)%, respectively.

In summary, the proposed model takes the input parameters of $v_{driving}$ and C_{out} as a function of time (t), and C_{in} at $t = 0$. With vehicle-specific leakage parameter data K_f and n from a cabin pressurization test, the model estimates C_{in} with respect to both time and driving speed for any vehicle models at any ventilation conditions.

Results and discussion

The results are presented in the following three sections. Model validation section describes the model validation. RC-mode air exchange rates section presents UFP I/O ratio changes under OA and RC modes to discuss passenger exposures. Passenger exposures section describes conditions that produce infiltration even with positive cabin pressurization under OA mode.

Model validation

Fig. 2 illustrates the comparison between the model predictions and the measurements at driving speeds ranging from 0 to 130 km/h for all simulation runs (one simulation per vehicle at medium fan setting over a range of speeds, 0 to 130 km/h). The model predictions agree well with the experimental data for UFPs ($R^2 = 0.78$) and even better for CO_2 ($R^2 = 0.83$). In Fig. 2, the slopes of the linear regressions are 1.56 for UFPs (Fig. 2a) and 1.14 for CO_2 (Fig. 2b), respectively.

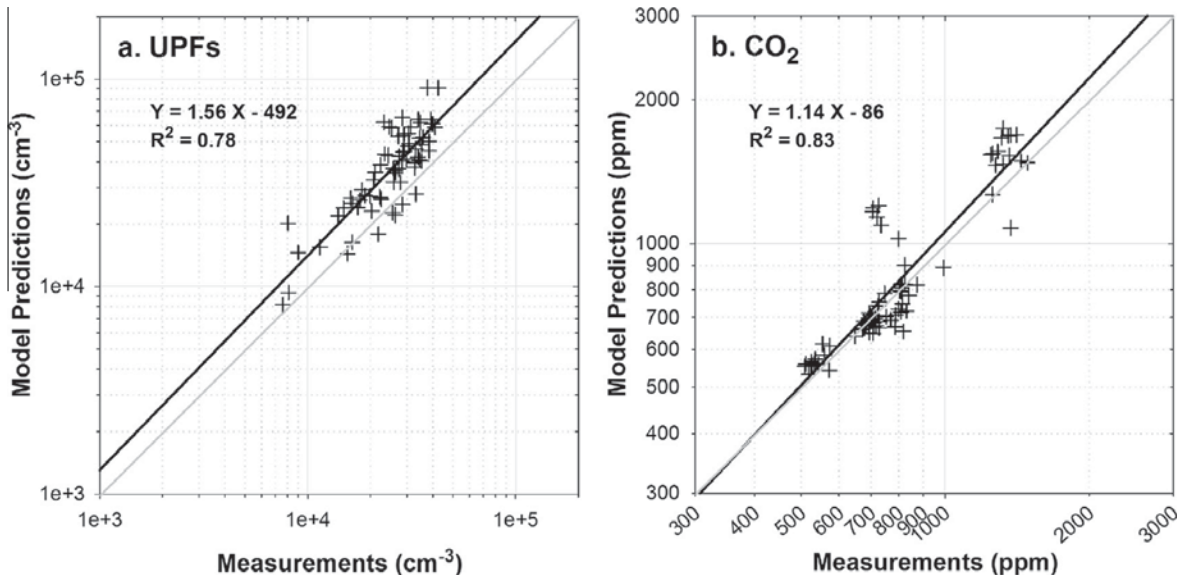

Fig. 2. The model estimations are compared to the measurements for (a) UFPs and (b) CO_2. The experimental validation data represents dynamic field conditions for a wide range of concentrations, driving speeds, ventilation settings, and different vehicle types.

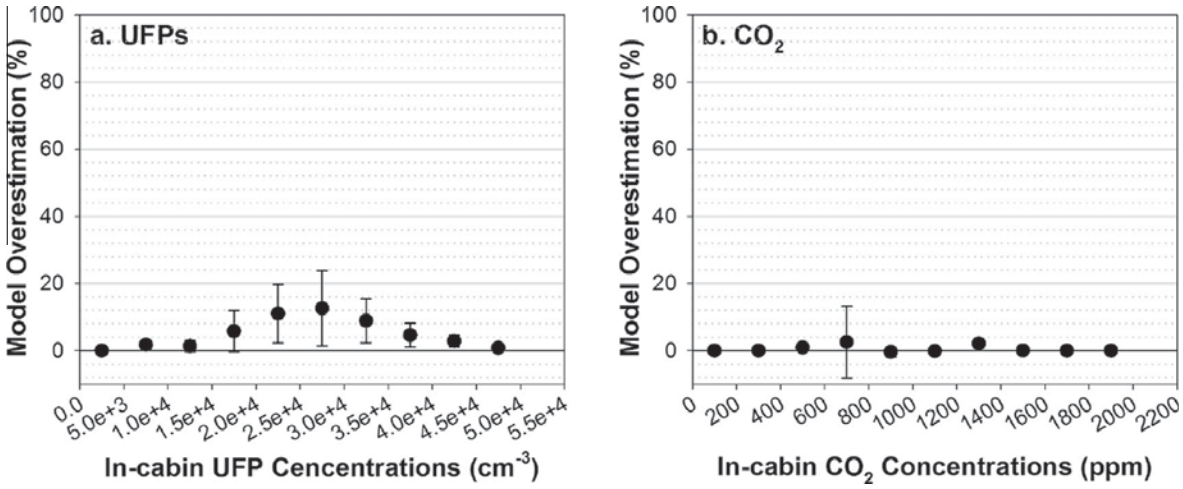

Fig. 3. Model discrepancy (black dots with error bars) is provided across the observed range of in-cabin concentrations for (a) UFPs and (b) CO_2.

Fig. 3 shows the difference between model prediction and observation, plotted as a percent overestimation in the given UFP and CO_2 concentration ranges. The plotted data are weighted by the number of observations in each concentration range. The in-cabin UFP concentration ranged widely from 7×10^3 to 5×10^4 cm^{-3}. However, a high UFP concentration (e.g., above 4.5×10^4 cm^{-3}) is less likely to occur in a typical in-cabin environment. Supporting information S2 shows the cumulative distributions of observed UFP and CO_2 concentrations, which are close to normal distributions. For example, the observation above 4.5×10^4 cm^{-3} only accounted for less than 1% of total observations in the passenger cabin. The Fig. 3 shows that the model overestimates the UPF concentration but predicts the CO_2 without bias. The average overall model overestimation was less than 16% throughout the range of observed particle numbers (Fig. 3a). For CO_2, the model discrepancy is less than 3% (Fig. 3b).

There are several possible causes for the over-prediction: evaporation, coagulation, and diffusion loss in the ventilation system. During data collection, the average in-cabin air conditions were 2 °C lower in temperature and 20% higher in relative humidity than the ambient air. Accordingly, particle evaporation is unlikely to make observable changes on the particle concentrations. As stated previously, the time required for coagulation is much longer than the particle residence time; therefore coagulation is not a likely cause for over-prediction. The most likely reason for over-prediction is particle loss in the ventilation ducts, which the model does not consider. Although the measurement data were collected for the same amount of time in stationary, local, and freeway conditions, a vast majority of high particle concentration data occurred during freeway driving. These particles are often dominated by nucleation-mode particles (i.e., mode diameter of ~20 nm). The smaller size of the particles can result in more Brownian diffusion, leading to higher deposition rates in ventilation ducts. This may explain why the absolute model discrepancy was greater at higher particle concentrations. Overall, the model provides reasonably good predictions with the model discrepancy less than 16% for UFPs under typical in-cabin conditions.

RC-mode air exchange rates

The proposed model is developed primarily to predict in-cabin UFP concentrations (i.e., C_{in}); but it can also estimate RC-mode AERs (AER_{atvRC}) with respect to driving speed. RC mode air exchange occurs only by infiltration; therefore, AER_{atvRC} is equal to Q_{inf}/V_{cabin} under well-mixed conditions. Fig. 4a compared the model predicted AER_{atvRC} with experimental measurements from previous studies as a function of driving speed (Engelmann et al., 1992; Knibbs et al., 2009; Ott et al., 2008; Park et al., 1998; Rodes et al., 1998). The modeling results for AER_{atvRC} are in reasonable agreement with experimental data in the literature. It should be noted, the test vehicles in the literature are different from the test vehicles in this study except for the 2005 Toyota Corolla (Ott et al., 2008).

Specific to the 2005 Toyota Corolla, Fig. 4b shows that the model predictions correspond well with the experimental observations from Ott et al. (2008) for the same vehicle model at the same driving speed in spite of the vehicle age differences. Previously, Fruin et al. (2011) statistically derived an AER_{atvRC} model which uses input parameters such as vehicle age and manufacturer. Both Fruin's and currently developed models predict that AER_{atvRC} increases exponentially at increasing driving speeds and agreed well with each other.

However, this study observed that the predicted AER_{atvRC} for individual vehicle could be different, presumably because automotive envelope leakage is more specific to manufacturer's design changes in vehicle model rather than the actual vehicle age. For instance, at 60 km/h, the AER_{atvRC} in this study were 5.8 and 8.1 h^{-1} for the 2001 and 2011 models of the Honda Accord, respectively (data not shown for clarity). At the same driving speed, the Fruin's model provided corresponding values of 8.2 and 4.4 h^{-1}, respectively.

Potential causes of these differences may be due to the nature of the different approaches. The previous AER_{atvRC} model was derived from statistical regressions assuming that the vehicle age has significant effects on AER_{atvRC}. Whereas, the

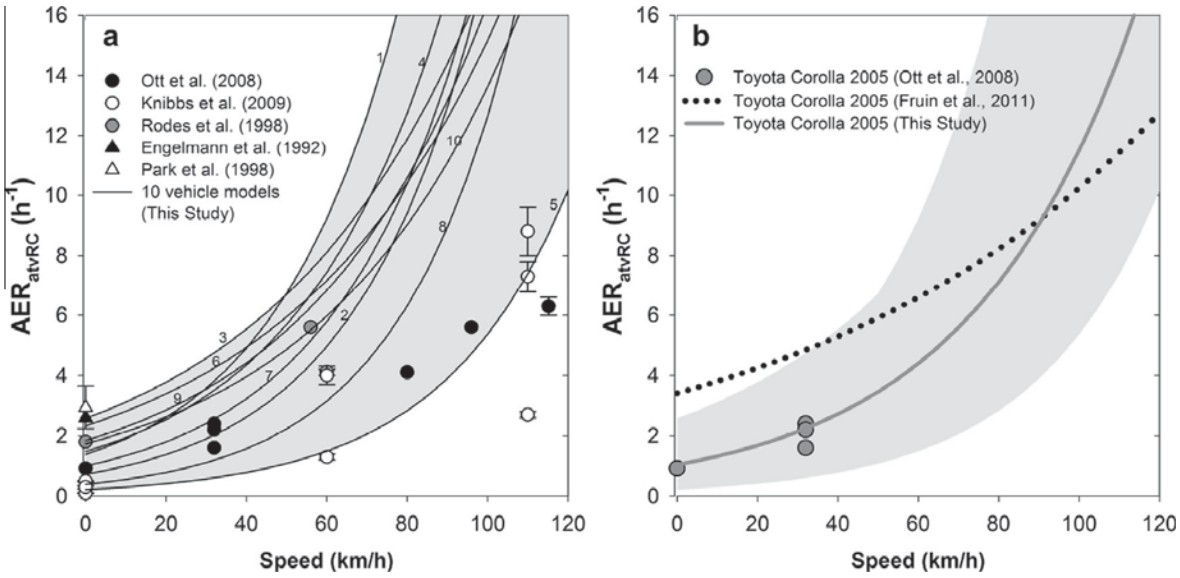

Fig. 4. The model estimated RC-mode air exchange rates (AER_{atvRC}) (solid lines in panel a) are plotted as a function of driving speed and compared to the measurement data from previous studies. The numbers next to the solid lines (in the panel a) refer to vehicle IDs listed in Table 2. AER_{atvRC} of a specific vehicle model/year are also compared to the measurement data from Ott et al. (2008) and model predictions from Fruin et al. (2011) in the panel b.

AER_{atvRC} estimated in this study depends on the physical properties of envelope leakage, such as the infiltration flow coefficient (K_f) and the pressure exponent (n) because AER_{atvRC} is driven by infiltration through the leakage. When considering manufacturers' design changes, the two leakage properties could also change AER_{atvRC} substantially and could become more specific to the vehicle model rather than vehicle age. Although vehicle aging can result in additional leakage, it is also important to consider the design changes in the vehicle models.

Passenger exposures

This modeling study quantified how much the infiltration can change UFP I/O under OA and RC mode ventilation conditions. Fig. 5 shows RC-mode simulation results for UFP I/O with respect to driving speed. Similarly, Fig. 6 shows OA-mode simulation results. Both simulations were conducted at three typical fan settings: fan-off (Q_{atvOA} = 0 m^3/h), the lowest (Q_{atvOA} = 100 m^3/h), and medium fan setting (Q_{atvOA} = 300 m^3/h). The fan conditions in model simulations were similar to the observation in 10 vehicle models: Q_{atvOA} = 97 m^3/h on average (±25 m^3/h) at the lowest fan setting and 306 m^3/h on average (±101 m^3/h) at the medium fan setting.

Recirculation mode

Under stationary conditions, RC-mode filtration can suppress UFP I/O by removing the infiltrated particles. Fig. 5b and c illustrate that the use of RC-mode filtration helps to reduce the overall I/O ratio. The I/O reduction by RC-mode filtration

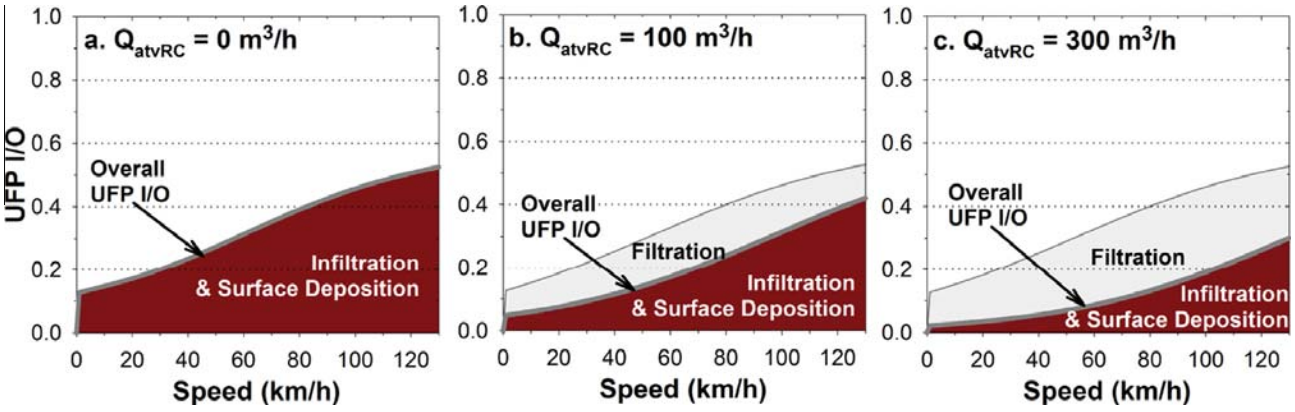

Fig. 5. Recirculation (RC) mode UFP I/O ratio increases at higher vehicle speeds. The model predictions are provided for Toyota Scion tC 2008 (see Lee et al., 2015) with ventilation airflow rates (i.e., Q_{atvRC}): (a) 0 m^3/h, (b) 100 m^3/h, and (c) 300 m^3/h. Different color schemes indicate different particle gain/loss mechanisms as noted.

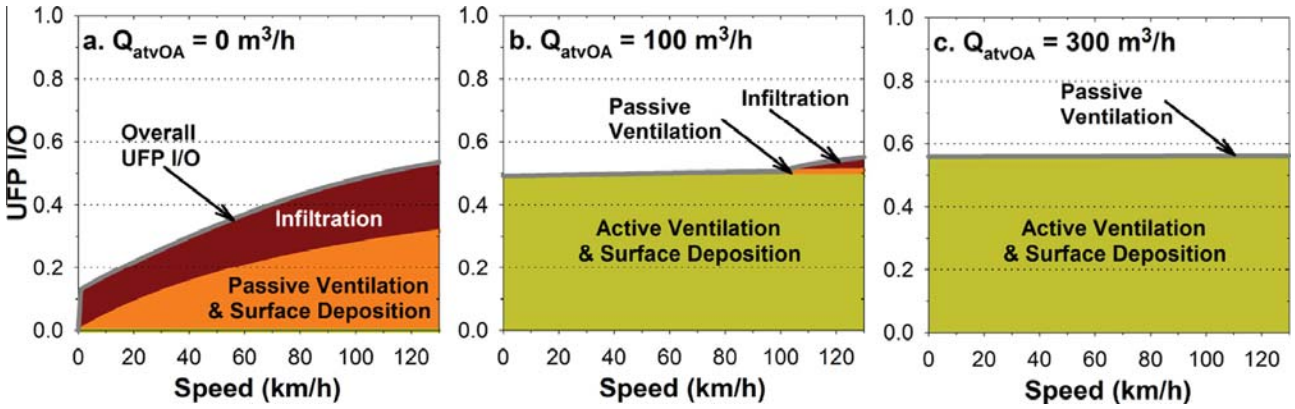

Fig. 6. Outdoor air (OA) mode UFP *I*/*O* ratio increases at higher vehicle speeds. The model predictions are provided for Toyota Scion tC 2008 (see Lee et al., 2015) with ventilation airflow rates (i.e., Q_{atvOA}): (a) 0 m^3/h, (b) 100 m^3/h, and (c) 300 m^3/h. Different color schemes indicate different particle gain/loss mechanisms as noted.

accounts for the difference between the overall UFP *I*/*O* with (Fig. 5b and c) and without (Fig. 5a) operating the filtration system. The developed model shows substantial decrease in UFP *I*/*O* below 0.05 (Fig. 5b) at the lowest fan setting and below 0.02 at the medium fan setting (Fig. 5c) under stationary conditions. These values are equivalent to 95% and 98% of in-cabin particle reduction (i.e., 1 − *I*/*O*), similar to the previous experimental findings (Pui et al., 2008).

When a vehicle is driving at higher speeds, UFP *I*/*O* can increase because of the infiltration. When the fan is off, UFP *I*/*O* is low (i.e., 0.12) in a stationary vehicle (Fig. 5a). However, at increasing driving speeds, the UFP *I*/*O* substantially increases up to 0.53 solely by infiltration. Similar patterns were also observed in other fan settings. For all fan settings, the overall *I*/*O* ratio increased due to excessive infiltration under high-speed driving conditions.

The RC-mode filtration is an effective particle removal process when taking into account in-cabin and on-road concentrations (i.e., 1 − *I*/*O*). However, its intrinsic efficiency can be much lower. Throughout the modeled driving speed range, RC-mode filtration only accounts for 44% and 69% removal of the infiltrated particles at the lowest and medium fan settings, respectively. Higher driving speed increased infiltration and reduced the intrinsic efficiency of UFP filtration. For instance, at the medium fan setting (Fig. 5c), the RC-mode filtration removes 87% of the infiltrated particles inside the passenger cabin at 0 km/h, but only 43% at 130 km/h.

Outdoor air mode

OA-mode ventilation can mitigate the effects from infiltration but still cannot prevent UFP *I*/*O* increase at higher vehicle speeds. Fig. 6 demonstrates OA-mode simulation results under the same fan condition. Using a fan setting of zero (Fig. 6a), infiltration and passive ventilation contribute 49% and 51% of total in-cabin UFPs. However, Fig. 6c illustrates that the use of medium fan setting stabilizes UFP *I*/*O* for a given driving speed although the passive ventilation slightly increase the *I*/*O*. The use of medium fan setting diminishes the contributions of infiltration (0%) and passive ventilation (0.3%) to the total in-cabin UFPs (Fig. 6c).

Different particle transport mechanisms can affect overall passenger exposure level of different magnitudes. For example, when the fan is off (Fig. 6a), infiltration and passive ventilation can substantially increase the UFP *I*/*O* from 0.15 at 0 km/h to 0.57 at 130 km/h. Note that the UFP *I*/*O* under OA mode (Fig. 6a) is different from under RC mode (Fig. 5a). Although the results are similar in magnitude, the simulation data were resulted from different pollutant transport mechanisms involved under different ventilation conditions.

In addition, even at the lowest fan setting (i.e., Q_{atvOA} = 100 m^3/h, Fig. 6b), UFP *I*/*O* still increased because of infiltration and passive ventilation, although the magnitude is relatively small (i.e., UFP *I*/*O* = 0.50 at 0 km/h and 0.57 at 130 km/h). The medium fan setting (Fig. 6c) keeps the overall UFP *I*/*O* at a constant level; however, this scenario results in the highest level of UFP *I*/*O* (i.e., 0.58). Therefore, the passenger exposure can become larger at higher fan setting under OA mode.

In summary, Figs. 5 and 6 demonstrate how different particle transport mechanisms can affect passenger exposures (i.e., UFP *I*/*O*). This study found that the UFP *I*/*O* generally increases as a function of driving speed. However, the magnitude of the *I*/*O* increase is a complex function of Q_{atvOA}, Q_{psvOA}, and Q_{inf}. Under RC mode (Fig. 5), infiltration is the dominant mechanism. Under OA mode (Fig. 6), its relation to the three mechanisms: infiltration, passive ventilation, and mechanical ventilation, is more complicated. Overall, the level of passenger exposure can increase at high driving speeds under both OA and RC modes. Although the medium fan setting stabilizes UFP *I*/*O* at almost constant level across the modeled speed range, the highest overall UFP *I*/*O* was found in this scenario under OA mode. Figs. 5 and 6 provided the modeling results from a representative vehicle to discuss the relative importance of different mechanisms affecting *I*/*O* ratios. The same conclusions can be reached for other vehicles except the *I*/*O* ratio will be different due to vehicle-specific input parameters (i.e., K_f, n, V_{cabin}, and Q_{atvOA}).

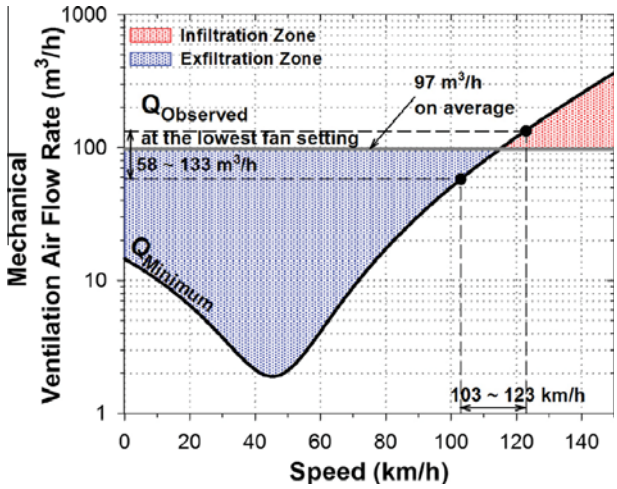

Fig. 7. Minimum ventilation airflow rate ($Q_{Minimum}$, solid black line) required to prevent infiltration under OA mode. The $Q_{Minimum}$ is compared to the observed ventilation flow rates ($Q_{Observed}$, solid gray line) at the lowest fan setting.

Infiltration under cabin pressurization

Infiltration can be prevented under the OA-mode cabin pressurization as seen in Fig. 6c. To investigate this further, the model was used to determine the minimum mechanical ventilation airflow rate ($Q_{Minimum}$) required to prevent infiltration. The $Q_{Minimum}$ is the average of model predictions for the vehicles listed in Table 2. The $Q_{Observed}$ is the average of observed mechanical ventilation airflow rate in the same vehicles. The $Q_{Minimum}$ and $Q_{Observed}$ are plotted in Fig. 7 and the range of $Q_{Observed}$ is given in dash-lines.

Infiltration occurs when $\Delta P_{inf} > 0$ in Eq (5), whereas it can be prevented by maintaining $\Delta P_{inf} \leqslant 0$. From this relationship, the critical Q_{atvOA} was estimated and is shown in Fig. 7 as $Q_{Minimum}$. Since Q_{psvOA} in Eq (5) is a function of driving speed, the $Q_{Minimum}$ changes across different speeds. The $Q_{Observed}$ was 97 m^3/h on average at the lowest fan setting and ranged from 58 to 133 m^3/h across the test vehicle models.

As shown in Fig. 7, the minimum required ventilation airflow rate (i.e., $Q_{Minimum}$) to prevent infiltration decreases until the driving speed increases to 45 km/h. When a vehicle is stationary, $Q_{Minimum}$ is approximately 10 m^3/h. At increasing speeds up to 45 km/h, $Q_{Minimum}$ is less than 10 m^3/h because passive ventilation (i.e., Q_{psvOA}) increases air supply through the open air damper. Above a driving speed of 45 km/h, a greater $Q_{Minimum}$ is required to prevent infiltration, and therefore greater mechanical ventilation (i.e., Q_{atvOA}) is necessary in addition to passive ventilation (i.e., Q_{psvOA}). $Q_{Minimum}$ increases to 200 m^3/h at 130 km/h. Therefore, higher driving speed requires more mechanical ventilation due to excessive infiltration.

Fig. 7 shows that the lowest average fan setting (i.e., Q_{atvOA} = 97 m^3/h on average for the 10 tested vehicles) can prevent the infiltration at driving speeds less than 103–123 km/h (115 km/h on average). Above that, a higher fan setting is needed. Even under OA-mode cabin pressurization, infiltration can occur at high driving speeds depending on the fan setting (i.e., Q_{atvOA}).

Model limitation and application

The proposed model is limited in predicting in-cabin pollutants other than UFPs and CO_2. The model needs to be validated for other types of particulate pollutants (e.g., black carbon and $PM_{2.5}$), which are also of significant health concerns in motor-vehicle environments. In addition, previous studies reported that engine/fuel system leaks may contribute to high levels of carcinogenic organic gas compounds (e.g., benzene, toluene, xylene, and methyl-tertiary butyl ether) in vehicle cabins (Duffy and Nelson, 1997; Faber et al., 2013; Fedoruk and Kerger, 2003; Jo and Park, 1998). The current model is limited to account for chemical reactions and secondary particle formations.

However, the proposed model is useful for in-depth analysis on passenger exposures because it enables pollutant transport mechanism-specific simulations. This model is also useful to determine the parameters that can significantly increase the level of passenger exposure to vehicular air pollution. As this study discussed, the relative importance of each parameter/transport mechanism can be significantly different in a wide range of driving speed, as well as, by selecting different ventilation modes (e.g., OA and RC modes). Furthermore, the proposed model can provide important information on what transport mechanism to control and under what condition. All of which are important to achieve an ultimate goal of reducing passenger exposures to vehicular air pollution.

Conclusions

This study incorporated infiltration and passive ventilation into a previously developed in-cabin air quality model. The infiltration term was formulated using Bernoulli's equation and the passive ventilation term was experimentally derived.

This mathematical model is different from the previous statistical models and enables vehicle-specific simulation. This new model provides transport mechanism-specific information and also provides the in-cabin particle/gas pollutant concentrations as a function of driving speed over time and under any automotive ventilation conditions (i.e., selection of OA/RC mode and blower fan setting). The overall model discrepancy remains less than 16% for UFPs and 3% for CO_2 in a typical range of in-cabin concentrations.

Using this new model, this study found that infiltration and passive ventilation are the reasons of increasing UFP I/O ratio at higher driving speeds. Although mechanical ventilation systems dominantly controlled the in-cabin air quality, especially at higher fan setting under OA mode, the infiltration and passive ventilation added more UFPs into the passenger cabin and consequently increased the I/O ratio. The UFP I/O ratio also increased under the RC mode because of infiltration mechanism alone. RC-mode filtration was effective in removing the in-cabin UFPs at lower driving speeds. At higher driving speeds, however, its effectiveness can substantially decrease due to excessive infiltration. The mechanical ventilation airflow rate at the lowest fan setting is sufficient to prevent infiltration at an averaged driving speed of 115 km/h or less; a greater fan speed is needed to provide higher cabin pressure and to prevent infiltration occurring above 115 km/h. This finding indicates infiltration can occur mostly under RC mode but can also occur under OA mode at high driving speeds.

Acknowledgments

This study complements work in progress supported by the National Science Foundation's CAREER Award under contract #32525-A6010 AI. Any opinions, findings, conclusions, or recommendations expressed in this report are those of the authors and do not necessarily reflect the views of the National Science Foundation.

Appendix A. Supplementary data

Supplementary data associated with this article can be found, in the online version, at http://dx.doi.org/10.1016/j.trd.2014.11.005.

References

Andersen, Z.J., Olsen, T.S., Andersen, K.K., Loft, S., Ketzel, M., Raaschou-Nielsen, O., 2010. Association between short-term exposure to ultrafine particles and hospital admissions for stroke in Copenhagen, Denmark. Eur. Heart J. 31 (16), 2034–2040.
Baker, P.H., Sharples, S., Ward, I.C., 1987. Air-flow through cracks. Build. Environ. 22 (4), 293–304.
Batchelor, G.K., 1967. An Introduction to Fluid Dynamics. Cambridge University Press, Cambridge, UK.
Duffy, B.L., Nelson, P.F., 1997. Exposure to emissions of 1,3-butadiene and benzene in the cabins of moving motor vehicles and buses in Sydney, Australia. Atmos. Environ. 31 (23), 3877–3885.
Elder, A., Couderc, J.-P., Gelein, R., Eberly, S., Cox, C., Xia, X., Zareba, W., Hopke, P., Watts, W., Kittelson, D., Frampton, M., Utell, M., Oberdorster, G., 2007. Effects of on-road highway aerosol exposures on autonomic responses in aged, spontaneously hypertensive rats. Inhalation Toxicol. 19 (1), 1–12.
Engelmann, R.J., Pendergrass, W.R., White, J.R., Hall, M.E., 1992. THE effectiveness of stationary automobiles as shelters in accidental releases of toxic materials. Atmos. Environ., Part A 26 (17), 3119–3125.
Faber, J., Brodzik, K., Golda-Kopek, A., Lomankiewicz, D., 2013. Benzene, toluene and xylenes levels in new and used vehicles of the same model. J. Environ. Sci. China 25 (11), 2324–2330.
Fedoruk, M.J., Kerger, B.D., 2003. Measurement of volatile organic compounds inside automobiles. J. Expo. Anal. Environ. Epidemiol. 13 (1), 31–41.
Fletcher, B., Saunders, C.J., 1994. Air change rates in stationary and moving motor-vehicles. J. Hazard. Mater. 38 (2), 243–256.
Fruin, S., Westerdahl, D., Sax, T., Sioutas, C., Fine, P.M., 2008. Measurements and predictors of on-road ultrafine particle concentrations and associated pollutants in Los Angeles. Atmos. Environ. 42 (2), 207–219.
Fruin, S.A., Hudda, N., Sioutas, C., Defino, R.J., 2011. Predictive model for vehicle air exchange rates based on a large, representative sample. Environ. Sci. Technol. 45 (8), 3569–3575.
Gong, L., Xu, B., Zhu, Y., 2009. Ultrafine particles deposition inside passenger vehicles. Aerosol Sci. Technol. 43 (6), 544–553.
Hinds, W.C., 1999. Aerosol Technology: Properties, Behavior, and Measurement of Airborne Particles, 2nd, ed. Wiley, New York.
Hudda, N., Eckel, S.R., Knibbs, L.D., Sioutas, C., Delfino, R.J., Fruin, S.A., 2012. Linking in-vehicle ultrafine particle exposures to on-road concentrations. Atmos. Environ. 59, 578–586.
Jo, W.K., Park, K.H., 1998. Exposure to carbon monoxide, methyl-tertiary butyl ether (MTBE), and benzene levels inside vehicles traveling on an urban area in Korea. J. Expo. Anal. Environ. Epidemiol. 8 (2), 159–171.
Joodatnia, P., Kumar, P., Robins, A., 2013. Fast response sequential measurements and modelling of nanoparticles inside and outside a car cabin. Atmos. Environ. 71, 364–375.
Kang, S.O., Jun, S.O., Park, H.I., Song, K.S., Kee, J.D., Kim, K.H., Lee, D.H., 2012. Actively translating a rear diffuser device for the aerodynamic drag reduction of a passenger car. Int. J. Automot. Technol. 13 (4), 583–592.
Knibbs, L.D., de Dear, R.J., Atkinson, S.E., 2009. Field study of air change and flow rate in six automobiles. Indoor Air 19 (4), 303–313.
Lee, E.S., Stenstrom, M.K., Zhu, Y.F., 2015. Ultrafine particles infiltration into passenger vehicles Part I: experimental evidences. Transp. Res. Part D.: Transp. Environ. 38, 156–165.
Lee, E.S., Zhu, Y.F., 2014. Application of a high-efficiency cabin air filter for simultaneous mitigation of ultrafine particle and carbon dioxide exposures inside passenger vehicles. Environ. Sci. Technol. 48 (4), 2328–2335.
Morawska, L., Ristovski, Z., Jayaratne, E.R., Keogh, D.U., Ling, X., 2008. Ambient nano and ultrafine particles from motor vehicle emissions: characteristics, ambient processing and implications on human exposure. Atmos. Environ. 42 (35), 8113–8138.
Ott, W., Klepeis, N., Switzer, P., 2008. Air change rates of motor vehicles and in-vehicle pollutant concentrations from secondhand smoke. J. Exp. Sci. Environ. Epidemiol. 18 (3), 312–325.
Park, J.H., Spengler, J.D., Yoon, D.W., Dumyahn, T., Lee, K., Ozkaynak, H., 1998. Measurement of air exchange rate of stationary vehicles and estimation of in-vehicle exposure. J. Exp. Anal. Environ. Epidemiol. 8 (1), 65–78.
Penttinen, P., Timonen, K.L., Tiittanen, P., Mirme, A., Ruuskanen, J., Pekkanen, J., 2001. Ultrafine particles in urban air and respiratory health among adult asthmatics. Eur. Respir. J. 17 (3), 428–435.
Peters, A., Wichmann, H.E., Tuch, T., Heinrich, J., Heyder, J., 1997. Respiratory effects are associated with the number of ultrafine particles. Am. J. Respir. Crit. Care Med. 155 (4), 1376–1383.

Pui, D.Y.H., Qi, C., Stanley, N., Oberdorster, G., Maynard, A., 2008. Recirculating air filtration significantly reduces exposure to airborne nanoparticles. Environ. Health Perspect. 116 (7), 863–866.
Rodes, C., Sheldon, L., Whitaker, D., Clayton, A., Fitzgerald, K., Flanagan, J., DiGenova, F., Hering, S., Frazier, C., 1998. Measuring concentrations of selected air pollutants inside California vehicles, Report prepared for California EPA. California Air Resources Board.
Shi, Z.B., Shao, L.Y., Jones, T.P., Whittaker, A.G., Lu, S.L., Berube, K.A., He, T., Richards, R.J., 2003. Characterization of airborne individual particles collected in an urban area, a satellite city and a clean air area in Beijing, 2001. Atmos. Environ. 37 (29), 4097–4108.
Sioutas, C., Delfino, R.J., Singh, M., 2005. Exposure assessment for atmospheric ultrafine particles (UFPs) and implications in epidemiologic research. Environ. Health Perspect. 113 (8), 947–955.
Somers, C.M., McCarry, B.E., Malek, F., Quinn, J.S., 2004. Reduction of particulate air pollution lowers the risk of heritable mutations in mice. Science 304 (5673), 1008–1010.
Song, K.S., Kang, S.O., Jun, S.O., Park, H.I., Kee, J.D., Kim, K.H., Lee, D.H., 2012. Aerodynamic design optimization of rear body shapes of a sedan for drag reduction. Int. J. Automot. Technol. 13 (6), 905–914.
Stolzel, M., Breitner, S., Cyrys, J., Pitz, M., Wolke, G., Kreyling, W., Heinrich, J., Wichmann, H.E., Peters, A., 2007. Daily mortality and particulate matter in different size classes in Erfurt, Germany. J. Exposure Sci. Environ. Epidemiol. 17 (5), 458–467.
Tartakovsky, L., Baibikov, V., Czerwinski, J., Gutman, M., Kasper, M., Popescu, D., Veinblat, M., Zvirin, Y., 2013. In-vehicle particle air pollution and its mitigation. Atmos. Environ. 64, 320–328.
von Klot, S., Wolke, G., Tuch, T., Heinrich, J., Dockery, D.W., Schwartz, J., Kreyling, W.G., Wichmann, H.E., Peters, A., 2002. Increased asthma medication use in association with ambient fine and ultrafine particles. Eur. Respir. J. 20 (3), 691–702.
Xu, B., Liu, S., Zhu, Y., 2010. Ultrafine particle penetration through idealized vehicle cracks. J. Aerosol Sci. 41 (9), 859–868.
Xu, B., Zhu, Y., 2009. Quantitative analysis of the parameters affecting in-cabin to on-roadway (I/O) ultrafine particle concentration ratios. Aerosol Sci. Technol. 43 (5), 400–410.
Zhu, Y.F., Eiguren-Fernandez, A., Hinds, W.C., Miguel, A.H., 2007. In-cabin commuter exposure to ultrafine particles on Los Angeles freeways. Environ. Sci. Technol. 41 (7), 2138–2145.